JOURNAL OF COMPUTATIONAL PHYSICS 115, 200–212 (1994)

Weighted Essentially Non-oscillatory Schemes

XU-DONG LIU,* STANLEY OSHER,† AND TONY CHAN‡

Department of Mathematics, UCLA, Los Angeles, California, 90024

Received December 7, 1992; revised April 18, 1994

In this paper we introduce a new version of ENO (essentially non-oscillatory) shock-capturing schemes which we call weighted ENO. The main new idea is that, instead of choosing the "smoothest" stencil to pick one interpolating polynomial for the ENO reconstruction, we use a convex combination of all candidates to achieve the essentially non-oscillatory property, while additionally obtaining one order of improvement in accuracy. The resulting weighted ENO schemes are based on cell averages and a TVD Runge–Kutta time discretization. Preliminary encouraging numerical experiments are given. © 1994 Academic Press, Inc.

1. INTRODUCTION

In this paper we present a new version of ENO (essentially non-oscillatory) schemes. The cell-average version of ENO schemes originally was introduced and developed by Harten and Osher in [1] and Harten, Engquist, Osher, and Chakravarthy in [2]. Later Shu and Osher developed the flux version of ENO schemes and introduced the TVD Runge–Kutta time discretization in [3, 4]. The ENO schemes work well in many numerical experiments. The new ENO schemes which we call the weighted ENO schemes are based on cell averages and the TVD Runge–Kutta time discretization.

The only difference between these schemes and the standard cell-average version of ENO is how we define a reconstruction procedure which produces a high-order accurate global approximation to the solution from its given cell averages. The cell-average version of ENO schemes attempts to avoid growth of spurious oscillations by an adaptive-stencil approach, in which each cell is assigned its own stencil of cells for the purposes of reconstruction. For each cell the cell-average version of ENO schemes selects an interpolating stencil in which the solution is smoothest in some sense. Thus a cell near a discontinuity is assigned a stencil from the smooth part of the solution and a Gibbs-like phenomenon is so avoided (see [5]). The weighted ENO schemes developed here follow this basic idea by using a convex combination approach, in which each cell is assigned all the corresponding stencils and a convex combination of all the corresponding interpolating polynomials on the stencils is computed to be the approximating polynomial. This is done by assigning proper weights to the convex combination. To achieve the essentially non-oscillatory property as the cell-average version of ENO, the weighted ENO schemes require that the convex combination be essentially a convex combination of the interpolating polynomials on the smooth stencils and that the interpolating polynomials on the discontinuous stencils have essentially no contribution to the convex combination. Thus, as in the cell-average version of ENO schemes, a cell near a discontinuity is essentially assigned stencils from the smooth part of the solution and a Gibbs-like phenomenon is also avoided. In addition to this, the convex combination approach results in the cancellation of truncation errors of corresponding interpolating polynomials and improves the order of accuracy by one. Another possible advantage of weighted ENO is smoother dependence on data which may lessen some of ENO's oscillatory behavior near convergence and may help in obtaining a convergence proof.

In Section 2 we introduce some notations and basic notions and give the TVD Runge–Kutta time discretization. In Section 3 we describe the procedure of reconstruction from given cell averages. In Section 4 we present some preliminary numerical experiments.

2. BASIC FORMULATION AND TVD RUNGE–KUTTA TIME DISCRETIZATION

We consider a hyperbolic conservation law

$$\begin{aligned} u_t + f(u)_x &= 0, \\ u(x, 0) &= u_0(x). \end{aligned} \tag{2.1}$$

Let $\{I_j\}$ be a partition of R, where $I_j = [x_{j-1/2}, x_{j+1/2}]$ is

* Research supported by NSF Grant DMS 91-04311.

† Research supported by NSF DMS 91-03104 and ONR NOO014-92-J-1890.

‡ Research supported by NSF ASC90-91-03002, ARO DAAL03-91-G-150, and ONR NOO014-90-J-1695.

0021-9991/94 $6.00

the jth cell, $x_{j+1/2}-x_{j-1/2}=h$. Denote $\{\bar{u}_j(\cdot,t)\}$ to be the sliding averages of the weak solution $u(x,t)$ of (2.1), i.e.,

$$\bar{u}_j(\cdot,t)=\frac{1}{h}\int_{I_j} u(x,t)\,dx. \tag{2.2}$$

Integrating (2.1) over each cell I_j, we obtain that the sliding averages $\{\bar{u}_j(\cdot,t)\}$ satisfy

$$\frac{\partial}{\partial t}\bar{u}_j(\cdot,t)=-\frac{1}{h}[f(u(x_{j+1/2},t))-f(u(x_{j-1/2},t))]. \tag{2.3}$$

To evaluate each $(\partial/\partial t)\,\bar{u}_j(\cdot,t)$, we need to evaluate $f(u(x,t))$ at each interface $x_{j+1/2}$. First, from the given cell averages $\bar{u}=\{\bar{u}_j\}$ in which $\bar{u}_j$ approximates $\bar{u}_j(\cdot,t)$, we reconstruct the solution to obtain $R(x)=\{R_j(x)\}$ which is a piecewise polynomial with uniform polynomial degree $r-1$, and in which each $R_j(x)$ is a polynomial approximating $u(x,t)$ on I_j. We shall show how to obtain $R(x)$ from $\bar{u}=\{\bar{u}_j\}$ in Section 3. Next, at each interface $x_{j+1/2}$, $R(x)$ may have two approximating values $R_j(x_{j+1/2})$ and $R_{j+1}(x_{j+1/2})$ for $u(x_{j+1/2},t)$. We need a two-point Lipschitz monotone flux $\tilde{h}(\cdot,\cdot)$ which is nondecreasing for the first argument and nonincreasing for the second argument. Some possible choices are

(i) *Engquist–Osher,*

$$h^{\mathrm{EO}}(a,b)=\int_0^b \min(f'(s),0)\,ds + \int_0^a \max(f'(s),0)\,ds + f(0); \tag{2.4}$$

(ii) *Godunov,*

$$h^{\mathrm{G}}(a,b)=\begin{cases}\min_{a\leqslant u\leqslant b} f(u) & \text{if } a\leqslant b,\\ \max_{a\geqslant u\geqslant b} f(u) & \text{if } a>b;\end{cases} \tag{2.5}$$

(iii) *Roe with entropy fix,*

$$h^{\mathrm{RF}}(a,b)=\begin{cases} f(a) & \text{if } f'(u)\geqslant 0 \text{ for } u\in[\min(a,b),\max(a,b)],\\ f(b) & \text{if } f'(u)\leqslant 0 \text{ for } u\in[\min(a,b),\max(a,b)],\\ h^{\mathrm{LLF}}(a,b) & \text{otherwise,}\end{cases} \tag{2.6a}$$

where $h^{\mathrm{LLF}}(a,b)$ is defined as

$$h^{\mathrm{LLF}}(a,b)=\tfrac{1}{2}[f(a)+f(b)-\beta(b-a)],\qquad \beta=\max_{\min(a,b)\leqslant u\leqslant\max(a,b)}|f'(u)|. \tag{2.6b}$$

We approximate $f(u(x_{j+1/2},t))$ by $\tilde{h}(R_j(x_{j+1/2}), R_{j+1}(x_{j+1/2}))$ and $f(u(x_{j-1/2},t))$ by $\tilde{h}(R_{j-1}(x_{j-1/2}), R_j(x_{j-1/2}))$. Therefore,

$$\frac{\partial}{\partial t}\bar{u}_j(\cdot,t)\approx L_j(\bar{u}), \tag{2.7a}$$

where

$$L_j(\bar{u})=-\frac{1}{h}[\tilde{h}(R_j(x_{j+1/2}),R_{j+1}(x_{j+1/2}))-\tilde{h}(R_{j-1}(x_{j-1/2}),R_j(x_{j-1/2}))]. \tag{2.7b}$$

In Section 3, in which we introduce the reconstruction procedure, we shall obtain that, in each cell I_j,

$$u(x,t)=R_j(x)+O(h^r)\qquad \forall x\in I_j, \tag{2.8}$$

and at one chosen point of two end points of I_j,

$$u(x_j^*,t)=R_j(x_j^*)+O(h^{r+1}),\qquad x_j^*=x_{j-1/2}\quad\text{or}\quad x_j^*=x_{j+1/2}. \tag{2.9}$$

Here and below we always consider smooth solutions when we discuss accuracy.

For general upwind schemes, away from sonic points (where $f'(u)=0$),

$$\tilde{h}(a,b)=\begin{cases}f(a) & \text{in the regions of } f'>0\\ f(b) & \text{in the regions of } f'<0.\end{cases}$$

In the regions of $f'>0$, from (2.7b),

$$L_j(\bar{u})=-\frac{1}{h}[f(R_j(x_{j+1/2}))-f(R_{j-1}(x_{j-1/2}))],$$

and if we choose $x_j^*=x_{j+1/2}$ and $x_j^*=x_{j-1/2}$ in (2.9), i.e.,

$$u(x_{j+1/2},t)=R_j(x_{j+1/2})+O(h^{r+1})$$
$$u(x_{j-1/2},t)=R_{j-1}(x_{j-1/2})+O(h^{r+1});$$

hence

$$\frac{\partial}{\partial t}\bar{u}_j(\cdot,t)=L_j(\bar{u})+O(h^{r+1}). \tag{2.10}$$

Similarly, we shall have the generalized formula (2.10) in the regions of $f'<0$ by choosing $x_j^*=x_{j-1/2}$ and $x_{j+1}^*=x_{j+1/2}$ in (2.9). This will be detailed in Section 3.4. As usual, in the regions around $f'=0$ (sonic points), we obtain

$$\frac{\partial}{\partial t}\bar{u}_j(\cdot,t)=L_j(\bar{u})+O(h^r).$$

For high order time discretization, because of (2.10), we need the $(r+1)$th order TVD Runge–Kutta time discretizations introduced by Shu and Osher in [3]. We need only to spell out the third- and fourth-order methods, which will be implemented in our numerical experiments:

For third order, $\forall j$,

$$\begin{aligned}
\bar{u}_j^{(0)} &= \bar{u}_j^n, \\
\bar{u}_j^{(1)} &= \bar{u}_j^{(0)} + L_j(\bar{u}^{(0)}) \\
\bar{u}_j^{(2)} &= \tfrac{3}{4}\bar{u}_j^{(0)} + \tfrac{1}{4}\bar{u}_j^{(1)} + \tfrac{1}{4}L_j(\bar{u}^{(1)}) \\
\bar{u}_j^{n+1} &= \tfrac{1}{3}\bar{u}_j^{(0)} + \tfrac{2}{3}\bar{u}_j^{(2)} + \tfrac{2}{3}L_j(\bar{u}^{(2)}).
\end{aligned}$$

For fourth order, $\forall j$,

$$\begin{aligned}
\bar{u}_j^{(0)} &= \bar{u}_j^n, \\
\bar{u}_j^{(1)} &= \bar{u}_j^{(0)} + L_j(\bar{u}^{(0)}) \\
\bar{u}_j^{(2)} &= \tfrac{1}{2}\bar{u}_j^{(0)} + \tfrac{1}{2}\bar{u}_j^{(1)} - \tfrac{1}{4}L_j(\bar{u}^{(0)}) + \tfrac{1}{2}L_j(\bar{u}^{(1)}) \\
\bar{u}_j^{(3)} &= \tfrac{1}{9}\bar{u}_j^{(0)} + \tfrac{2}{9}\bar{u}_j^{(1)} + \tfrac{2}{3}\bar{u}_j^{(2)} - \tfrac{1}{9}L_j(\bar{u}^{(0)}) \\
&\quad - \tfrac{1}{3}L_j(\bar{u}^{(1)}) + L_j(\bar{u}^{(2)}) \\
\bar{u}_j^{n+1} &= \tfrac{1}{3}\bar{u}_j^{(1)} + \tfrac{1}{3}\bar{u}_j^{(2)} + \tfrac{1}{3}\bar{u}_j^{(3)} + \tfrac{1}{6}L_j(\bar{u}^{(1)}) \\
&\quad + \tfrac{1}{6}L_j(\bar{u}^{(3)}).
\end{aligned}$$

To complete the construction of our schemes we form our novel reconstruction procedure.

3. RECONSTRUCTION PROCEDURE

3.1. *Purposes of Reconstruction*

In this section we present the reconstruction procedure. The $R(x)$ is required to satisfy

(i) In each cell I_j, $\forall x \in I_j$ and one chosen point $x_j^* \in I_j$, we have

$$R_j(x) = u(x, t) + O(h^r) \tag{3.1a}$$

and

$$R_j(x_j^*) = u(x_j^*, t) + O(h^{r+1}), \tag{3.1b}$$

where (3.1b) will lead to one order of improvement in accuracy; see Section 3.4 in this paper.

(ii) $R(x)$ has conservation form, i.e., $\forall j$,

$$\frac{1}{h}\int_{I_j} R_j(x)\,dx = \bar{u}_j. \tag{3.2}$$

(iii) Every $R_j(x)$ achieves the "ENO property" which will be specified later.

3.2. *Interpolation on Each Stencil*

Following the reconstruction procedure in [2], given the cell averages $\{\bar{u}_j\}$, we can immediately evaluate the point values of the solution's primitive function $W(x)$ at interfaces $\{W(x_{j+1/2})\}$, where the primitive function is defined as

$$W(x) = \int_{x_{j'-1/2}}^{x} u(x, t)\,dx, \tag{3.3}$$

where $x_{j'-1/2}$ could be any interface; hence

$$u(x, t) = W'(x) = \frac{d}{dx}W(x) \tag{3.4}$$

and obviously

$$W(x_{j+1/2}) = \sum_{i=j'}^{j} \bar{u}_i \cdot h. \tag{3.5}$$

To reconstruct the solution, we interpolate $W(x)$ on each stencil $S_j = (x_{j-r+1/2}, x_{j-r+3/2}, \ldots, x_{j+1/2})$ to obtain a polynomial $p_j(x)$, i.e.,

$$p_j(x_{l+1/2}) = W(x_{l+1/2}), \qquad l = j-r, \ldots, j.$$

Obviously the corresponding polynomial $p_j'(x)$ (with degree $r-1$) approximates the solution $u(x, t)$, i.e.,

$$u(x, t) = p_j'(x) + O(h^r) \qquad \forall x \in (x_{j-r+1/2}, x_{j+1/2});$$

see [2].

Also for each stencil $S_j = (x_{j-r+1/2}, x_{j-r+3/2}, \ldots, x_{j+1/2})$, we define an indicator of the smoothness IS_j of $u(x, t)$ on S_j as following: First we compute a table of differences of $\{\bar{u}_j\}$ on S_j,

$$\begin{aligned}
&\Delta[\bar{u}_{j-r+1}],\ \Delta[\bar{u}_{j-r+2}],\ \ldots,\ \Delta[\bar{u}_{j-1}], \\
&\Delta^2[\bar{u}_{j-r+1}],\ \Delta^2[\bar{u}_{j-r+2}],\ \ldots,\ \Delta^2[\bar{u}_{j-2}], \\
&\vdots \\
&\Delta^{r-1}[\bar{u}_{j-r+1}],
\end{aligned}$$

where

$$\begin{aligned}
\Delta[\bar{u}_l] &= \bar{u}_{l+1} - \bar{u}_l \\
\Delta^k[\bar{u}_l] &= \Delta^{k-1}[\bar{u}_{l+1}] - \Delta^{k-1}[\bar{u}_l].
\end{aligned}$$

Next we define IS_j to be the summation of all averages of square values of the same order differences,

$$IS_j = \sum_{l=1}^{r-1}\left(\sum_{k=1}^{l}(\Delta^{r-l}[u_{j-r+k}])^2\right)\Big/ l.$$

That is, for $r=2$,

$$IS_j=[\Delta[u_{j-1}])^2;$$

and, for $r=3$,

$$IS_j=((\Delta[u_{j-2}])^2+(\Delta[u_{j-1}])^2)/2+(\Delta^2[u_{j-2}])^2.$$

We observe that if $u(x, t)$ is discontinuous on S_j, $IS_j\approx O(1)$, and if $u(x, t)$ is continuous on S_j, $IS_j\approx O(h^2)$. Hence for each stencil S_j, we obtain $p_j'(x)$ approximating $u(x, t)$ on S_j and IS_j indicating the smoothness of $u(x, t)$ on S_j.

In the following subsection, to reconstruct the solution in I_j, we shall use r interpolating polynomials $\{p'_{j+k}(x)\}_{k=0}^{r-1}$ on the stencils $\{S_{j+k}\}_{k=0}^{r-1}$, in which all S_{j+k} cover the I_j, to obtain a convex combination of them, and we shall explore $\{IS_{j+k}\}_{k=0}^{r-1}$ to assign a proper weight for each of $\{p'_{j+k}(x)\}_{k=0}^{r-1}$ in the convex combination for the purposes of reconstruction.

3.3. *Convex Combination of* $\{p'_{j+k}(x)\}_{k=0}^{r-1}$ *for Each Cell* I_j

For each cell I_j we have r stencils $\{S_{j+k}\}_{k=0}^{r-1}=\{(x_{j+k-r+1/2},\ x_{j+k-r+3/2},\ ...,\ x_{j+k+1/2})\}_{k=0}^{r-1}$ which all include two end points $x_{j-1/2}$ and $x_{j+1/2}$ of I_j. We also have r interpolating polynomials $\{p'_{j+k}(x)\}_{k=0}^{r-1}$ on the corresponding stencils $\{S_{j+k}\}_{k=0}^{r-1}$. The main idea of the cell-average version of ENO is to choose the "smoothest" one from these r interpolating polynomials. For weighted ENO, instead of choosing one, we use all r interpolating polynomials and compute a convex combination of them to obtain a polynomial $R_j(x)$ as

$$R_j(x)=\sum_{k=0}^{r-1}\frac{\alpha_k^j}{\sum_{l=0}^{r-1}\alpha_l^j}p'_{j+k}(x), \tag{3.6}$$

where the $\alpha_k^j>0$ $(k=0, 1, 2, ..., r-1)$. Obviously $u(x, t)=R_j(x)+O(h^r)$ in the smooth regions of $u(x, t)$ which is the purpose of (3.1a). Note that for any $k=0, 1, ..., r-1$, $p_{j+k}(x_{j-1/2})=W(x_{j-1/2})$ and $p_{j+k}(x_{j+1/2})=W(x_{j+1/2})$; hence we achieve the purpose of (3.2):

$$\begin{aligned}\frac{1}{h}\int_{I_j}R_j(x)\,dx&=\frac{1}{h}\sum_{k=0}^{r-1}\frac{\alpha_k^j}{\sum_{l=0}^{r-1}\alpha_l^j}(p_{j+k}(x_{j+1/2})-p_{j+k}(x_{j-1/2}))\\&=\frac{1}{h}\{W(x_{j+1/2})-W(x_{j-1/2})\}\\&\quad\times\sum_{k=0}^{r-1}\frac{\alpha_k^j}{\sum_{l=0}^{r-1}\alpha_l^j}=\bar{u}_j.\end{aligned} \tag{3.7}$$

Note that no matter how we define $\{\alpha_k^j\}_{k=0}^{r-1}$, $R_j(x)$ satisfies the purposes of (3.1a) and (3.2).

We specify the "ENO property" of $R_j(x)$ by the corresponding $\{\alpha_k^j\}_{k=0}^{r-1}$.

DEFINITION 1. The $R_j(x)$ has the "ENO property" if the corresponding $\{\alpha_k^j\}_{k=0}^{r-1}$ satisfy that

(i) If the stencil S_{j+k} is in the smooth regions, the corresponding α_k^j satisfy

$$\frac{\alpha_k^j}{\sum_{l=0}^{r-1}\alpha_l^j}=O(1). \tag{3.8a}$$

(ii) If the stencil S_{j+k} is in a discontinuous region of the solution $u(x, t)$, the corresponding α_k^j satisfy

$$\frac{\alpha_k^j}{\sum_{l=0}^{r-1}\alpha_l^j}\leqslant O(h^r). \tag{3.8b}$$

Note that, if $\{\alpha_k^j\}_{k=0}^{r-1}$ satisfy the "ENO property" (3.8),

$$R_j(x)=\sum_{k=0}^{r-1}\frac{\alpha_k^j}{\sum_{l=0}^{r-1}\alpha_l^j}p'_{j+k}(x)$$

will be a convex combination of the interpolating polynomials on the smooth stencils (3.8a) and the interpolating polynomials on the discontinuous stencils have essentially no contribution to $R_j(x)$ (3.8b).

Define,

$$\alpha_k^j=C_k^j/(\varepsilon+IS_{j+k})^r,\qquad k=0, ..., r-1, \tag{3.9}$$

where $C_k^j=O(1)$ and $C_k^j>0$ will be defined later for improvement of the accuracy. Note that because IS_{j+k} could be zero and $1/x$ is too sensitive as x is near zero, we add a small positive number $\varepsilon=10^{-5}$ in the denominator. Note that if the stencil S_{j+k} is in the smooth regions,

$$\frac{\alpha_k^j}{\sum_{l=0}^{r-1}\alpha_l^j}=O(1),$$

and if the stencil S_{j+k} is in the discontinuous regions of $u(x, t)$,

$$\frac{\alpha_k^j}{\sum_{l=0}^{r-1}\alpha_l^j}\leqslant\max(O(\varepsilon^r), O(h^{2r})).$$

Hence these $\{\alpha_k^j\}_{k=0}^{r-1}$ (3.9) satisfy the "ENO property" (3.8) $(O(\varepsilon^r)\leqslant O(10^{-10}))$. Here we assume there is at least one stencil of $\{S_{j+k}\}_{k=0}^{r-1}$ in the smooth regions.

No matter how we define the constants $\{C_k^j\}_{k=0}^{r-1}$, we have achieved the purposes of (3.1a), (3.2), and the "ENO property" (3.8). However, we shall specify $\{C_k^j\}_{k=0}^{r-1}$ for (3.1b) which will lead to one order of improvement in accuracy in Section 3.4, our last purpose of the reconstruction.

For our analysis we assume that

$$u(x, t) \in C^{r+1}, \tag{3.10}$$

in $[x_{j-r+1/2}, x_{j+r+1/2}]$.

For each $p'_{j+k}(x)$, we express its truncation error as

$$\begin{aligned} e_{j+k}(x) &= u(x, t) - p'_{j+k}(x) = W'(x) - p'_{j+k}(x) \\ &= \frac{d}{dx}\{W[x, x_{j+k-r+1/2}, \ldots, x_{j+k+1/2}] \\ &\quad \cdot \prod_{l=0}^{r} (x - x_{j+k-l+1/2})\} \\ &= \frac{d}{dx} W[x, x_{j+k-r+1/2}, \ldots, x_{j+k+1/2}] \\ &\quad \cdot \prod_{l=0}^{r} (x - x_{j+k-l+1/2}) \\ &\quad + W[x, x_{j+k-r+1/2}, \ldots, x_{j+k+1/2}] \\ &\quad \cdot \sum_{s=0}^{r} \left\{ \prod_{l=0, l\neq s}^{r} (x - x_{j+k-l+1/2}) \right\} \\ &= W[x, x_{j+k-r+1/2}, \ldots, x_{j+k+1/2}] \\ &\quad \cdot a_k^j(x) + O(h^{r+1}), \end{aligned} \tag{3.11a}$$

where $a_k^j(x) = \sum_{s=0}^{r} \{\prod_{l=0, l\neq s}^{r} (x - x_{j+k-l+1/2})\}$.

We express the truncation error for $R_j(x)$,

$$\begin{aligned} E_j(x) &= u(x, t_n) - R_j(x) = W'(x) - R_j(x) \\ &= \sum_{k=0}^{r-1} \frac{\alpha_k^j}{\sum_{l=0}^{r-1} \alpha_l^j} (W'(x) - p'_{j+k}(x)) \\ &= \sum_{k=0}^{r-1} \frac{\alpha_k^j}{\sum_{l=0}^{r-1} \alpha_l^j} e_{j+k}(x). \end{aligned}$$

Because of the assumption (3.10), $\forall k = 0, 1, \ldots, r-1$,

$$\begin{aligned} &|IS_{j+k}| \leqslant O(h^2) \\ &|IS_{j+k} - IS_j| \leqslant O(h^2) \\ &|a_k^j(x)| \leqslant O(h^r) \\ &|W[x, x_{j+k-r+1/2}, \ldots, x_{j+k+1/2}] \\ &\quad - W[x, x_{j-r+1/2}, \ldots, x_{j+1/2}]| \leqslant O(h). \end{aligned} \tag{3.11b}$$

We have, from (3.11a) and (3.11b),

$$\begin{aligned} E_j(x) &= \sum_{k=0}^{r-1} \frac{\alpha_k^j}{\sum_{l=0}^{r-1} \alpha_l^j} e_{j+k}(x) \\ &= \sum_{k=0}^{r-1} \frac{\alpha_k^j}{\sum_{l=0}^{r-1} \alpha_l^j} W[x, x_{j+k-r+1/2}, \ldots, x_{j+k+1/2}] \\ &\quad \cdot a_k^j(x) + O(h^{r+1}) \\ &= \left\{ \sum_{k=0}^{r-1} \frac{C_k^j}{\sum_{l=0}^{r-1} C_k^j} a_k^j(x) \right\} \cdot W[x, x_{j-r+1/2}, \ldots, x_{j+1/2}] \\ &\quad + O(h^{r+1}). \end{aligned} \tag{3.11c}$$

The idea is that for one chosen point $x_j^* \in [x_{j-1/2}, x_{j+1/2}]$, we define C_k^j to make the first term in (3.11c) equal to zero and obtain

$$E_j(x_j^*) = O(h^{r+1}).$$

For $x_j^* \in [x_{j-1/2}, x_{j+1/2}]$, we denote η_p as the number of positive terms in $\{a_k^j(x_j^*)\}_{k=0}^{r-1}$ and η_n as the number of negative terms in $\{a_k^j(x_j^*)\}_{k=0}^{r-1}$; then we define

$$C_k^j = \begin{cases} 1 & \text{if } a_k^j(x_j^*) = 0, \\ \dfrac{h^r}{\eta_p |a_k^j(x_j^*)|} & \text{if } a_k^j(x_j^*) > 0, \\ \dfrac{h^r}{\eta_n |a_k^j(x_j^*)|} & \text{if } a_k^j(x_j^*) < 0. \end{cases} \tag{3.12}$$

Obviously the C_k^j are independent of grid size h:

$$\begin{aligned} E_j(x_j^*) &= \left\{ \sum_{k=0}^{r-1} \frac{C_k^j}{\sum_{l=0}^{r-1} C_k^j} a_k^j(x_j^*) \right\} W[x, x_{j-r+1/2}, \ldots, x_{j+1/2}] \\ &\quad + O(h^{r+1}) \\ &= \left\{ \sum_{a_k^j(x_j^*)>0} \frac{1/\eta_p}{\sum_{l=0}^{r-1} C_l^j} - \sum_{a_k^j(x_j^*)<0} \frac{1/\eta_n}{\sum_{l=0}^{r-1} C_l^j} \right\} \\ &\quad \times W[x, x_{j-r+1/2}, \ldots, x_{j+1/2}] + O(h^{r+1}) \\ &= 0 + O(h^{r+1}) \\ &= O(h^{r+1}). \end{aligned} \tag{3.13}$$

Remark 1. We have to have $\eta_p \geqslant 1$ and $\eta_n \geqslant 1$ to guarantee (3.13).

Thus we obtain that, for one chosen point x_j^* and any other point $x \in [x_{j-1/2}, x_{j+1/2}]$, defining C_k^j by (3.12) gives us

$$E_j(x) = O(h^r) \tag{3.14a}$$

and

$$E_j(x_j^*) = O(h^{r+1}). \tag{3.14b}$$

Up to now, we have achieved all purposes of reconstruction (3.1a), (3.1b), (3.2), and (3.8).

3.4. *One Order of Improvement in Accuracy Using* (3.1b)

In this subsection, we shall see how (3.1b) or (3.14b) gives us one order of improvement in accuracy by choosing x_j^* properly in each cell. Let us consider the numerical spatial approximation (2.7b)

$$L_j(\bar{u}) = -\frac{1}{h}\left[\tilde{h}^{(R)}(x_{j+1/2}), R_{j+1}(x_{j+1/2})\right) - \tilde{h}(R_{j-1}(x_{j-1/2}), R_j(x_{j-1/2}))].$$

Consider three cells in a smooth region, say cells I_{j-1}, I_j, and I_{j+1}, which are away from sonic points.

If $f'(R(x)) > 0$ in the cells, we have

$$L_j(\bar{u}) = -\frac{1}{h}[f(R_j(x_{j+1/2})) - f(R_{j-1}(x_{j-1/2}))].$$

In (3.1b), we chose $x_j^* = x_{j+1/2}$ and $x_{j-1}^* = x_{j-1/2}$, then by (3.14b) we obtain that

$$R_j(x_{j+1/2}) - u(x_{j+1/2}, t) = E_j(x_{j+1/2}) = O(h^{r+1}),$$
$$R_{j-1}(x_{j-1/2}) - u(x_{j-1/2}, t) = E_{j-1}(x_{j-1/2}) = O(h^{r+1}).$$

Thus

$$L_j(\bar{u}) = -\frac{1}{h}[f(u(x_{j+1/2}, t)) - f(u(x_{j-1/2}, t))] + O(h^{r+1}).$$

If $f'(R(x)) < 0$ in the cells, we have

$$L_j(\bar{u}) = -\frac{1}{h}[f(R_{j+1}(x_{j+1/2})) - f(R_j(x_{j-1/2}))].$$

In (3.1b), we chose $x_j^* = x_{j-1/2}$ and $x_{j+1}^* = x_{j+1/2}$, then by (3.14b) we obtain that

$$R_{j+1}(x_{j+1/2}) - u(x_{j+1/2}, t) = E_{j+1}(x_{j+1/2}) = O(h^{r+1}),$$
$$R_j(x_{j-1/2}) - u(x_{j-1/2}, t) = E_j(x_{j-1/2}) = O(h^{r+1}).$$

Thus

$$L_j(\bar{u}) = -\frac{1}{h}[f(u(x_{j+1/2}, t)) - f(u(x_{j-1/2}, t))] + O(h^{r+1}).$$

Hence in the smooth regions and away from sonic points, the numerical spatial operators $\{L_j(\bar{u})\}$ approximate $\{(\partial/\partial t)\,\bar{u}_j(\cdot, t)\}$ to the order $O(h^{r+1})$.

We specify x_j^* in each I_j in the following way: *First we compute* $f'(\bar{u}_j)$. *Then*

(i) *if* $f'(\bar{u}_j) > 0$ *we chose* $x_j^* = x_{j+1/2}$,

(ii) *if* $f'(\bar{u}_j) < 0$ *we chose* $x_j^* = x_{j-1/2}$,

(iii) *if* $f'(\bar{u}_j) = 0$ *we chose* $x_j^* = x_{j+1/2}$ *or* $x_j^* = x_{j-1/2}$.

In the cell I_j is in the smooth regions and away from sonic points, then in general $f'(R(x)) \cdot f'(\bar{u}_j) > 0$ around the cell I_j; hence according to the above analysis

$$\frac{\partial}{\partial t}\bar{u}_j(\cdot, t) = L_j(\bar{u}) + O(h^{r+1}). \tag{3.15}$$

Because sonic points are isolated, in general, we obtain (3.15) in most of the cells and obtain

$$\frac{\partial}{\partial t}\bar{u}_j(\cdot, t) = L_j(\bar{u}) + O(h^r)$$

in a bounded, in fact small, number of cells near which there are sonic points as h decreases to zero.

Remark 2. We have achieved one order of improvement in accuracy. For $r = 2$ and $r = 3$ the cost of computing of the weighted ENO schemes is comparable to (of course, a little more expensive than) that of standard ENO schemes (with the same order of accuracy) on sequential computers. However, on parallel computers, to achieve the same order of accuracy, the former schemes are much less expensive than the latter because the latter need more expensive data transport between cells.

3.5. *Schemes for* $r = 2$

The purpose of the following two subsections 35. and 3.6 is to spell out the details of the general schemes for two specific values of r, perhaps to aid the reader in implementation.

In this subsection, we consider our schemes when $r = 2$. In this case we use linear interpolation to achieve the "ENO property" and third-order accuracy (in our numerical experiments, we achieved fourth-order accuracy) with conservation form.

Here we give the reconstruction procedure for $r = 2$. For each cell I_j, we have two stencils $S_j = (x_{j-3/2}, x_{j-1/2}, x_{j+1/2})$ and $S_{j+1} = (x_{j-1/2}, x_{j+1/2}, x_{j+3/2})$ corresponding to $I_j = [x_{j-1/2}, x_{j+1/2}]$. On these two stencils, we obtain two linear interpolations

$$p_j^1(x) = \bar{u}_j + \frac{\bar{u}_j - \bar{u}_{j-1}}{h}(x - x)$$

and

$$p_{j+1}^1(x) = \bar{u}_j + \frac{\bar{u}_{j+1} - \bar{u}_j}{h}(x - x_j),$$

and two indicators of smoothness $IS_j=(\bar{u}_j-\bar{u}_{j-1})^2$ and $IS_{j+1}=(\bar{u}_{j+1}-\bar{u}_j)^2$. The reconstructed solution $R_j(x)$ will be a convex combination of $p_j'(x)$ and $p_{j+1}^*(x)$, i.e.,

$$R_j(x)=\frac{\alpha_0^j}{\alpha_0^j+\alpha_0^j}p_j'(x)+\frac{\alpha_1^j}{\alpha_0^j+\alpha_1^j}p_{j+1}'(x), \tag{3.16}$$

where $\alpha_0^j=C_0^j/(\varepsilon+IS_j)^2$ and $\alpha_1^j=C_1^j/(\varepsilon+IS_{j+1})^2$. We shall specify C_0^j and C_1^j in the following two cases.

Case 1. If $f'(\bar{u}_j)>0$, we choose $x_j^*=x_{j+1/2}$. We compute $a_0^j(x_{j+1/2})=2h^2$ and $a_1^j(x_{j+1/2})=-h^2$ and obtain $\eta_p=1$ and $\eta_n=1$, hence $C_0^j=\frac{1}{2}$ and $C_1^j=1$. Thus

$$\begin{aligned}\alpha_0^j&=\frac{1}{2(\varepsilon+IS_j)^2}\\ \alpha_1^j&=\frac{1}{(\varepsilon+IS_{j+1})^2}\end{aligned} \tag{3.17a}$$

in (3.16).

Case 2. If $f'(\bar{u}_j)\leqslant 0$, we choose $x_j^*=x_{j-1/2}$. We compute $a_0^j(x_{j-1/2})=-h^2$ and $a_1^j(x_{j-1/2})=2h^2$ and obtain $\eta_p=1$ and $\eta_n=1$; hence $C_0^j=1$ and $C_1^j=\frac{1}{2}$. Thus

$$\begin{aligned}\alpha_0^j&=\frac{1}{(\varepsilon+IS_j)^2}\\ \alpha_1^j&=\frac{1}{2(\varepsilon+IS_{j+1})^2}\end{aligned} \tag{3.17b}$$

in (3.16).

3.6. *Schemes for* $r=3$

In this subsection, we consider our schemes when $r=3$. In this case we use quadratic interpolation to achieve the "ENO property" and fourth-order accuracy (in our numerical experiments, we achieve fifth-order accuracy) with the conservation form.

Here we give the reconstruction procedure for $r=3$. For each I_j, we have three stencils $S_j=(x_{j-5/2}, x_{j-3/2}, x_{j-1/2}, x_{j+1/2})$, $S_{j+1}=(x_{j-3/2}, x_{j-1/2}, x_{j+1/2}, x_{j+3/2})$, and $S_{j+2}=(x_{j-1/2}, x_{j+1/2}, x_{j+3/2}, x_{j+5/2})$ corresponding to $I_j=[x_{j-1/2}, x_{j+1/2}]$. On these three stencils, we obtain three quadratic interpolations

$$\begin{aligned}p_j(x)=&\frac{\bar{u}_j-2\bar{u}_{j-1}+\bar{u}_{j-2}}{2h^2}(x-x_{j-1})^2\\ &+\frac{\bar{u}_j-\bar{u}_{j-2}}{2h}(x-x_{j-1})\\ &+\bar{u}_{j-1}-\frac{\bar{u}_j-2\bar{u}_{j-1}+\bar{u}_{j-2}}{24}\end{aligned}$$

$$\begin{aligned}p_{j+1}'(x)=&\frac{\bar{u}_{j+1}-2\bar{u}_j+\bar{u}_{j-1}}{2h^2}(x-x_j)^2\\ &+\frac{\bar{u}_{j+1}-\bar{u}_{j-1}}{2h}(x-x_j)\\ &+\bar{u}_j-\frac{\bar{u}_{j+1}-2\bar{u}_j+\bar{u}_{j-1}}{24}\end{aligned}$$

and

$$\begin{aligned}p_{j+2}'(x)=&\frac{\bar{u}_{j+2}-2\bar{u}_{j+1}+\bar{u}_j}{2h^2}(x-x_{j+1})^2\\ &+\frac{\bar{u}_{j+2}-\bar{u}_j}{2h}(x-x_{j+1})\\ &+\bar{u}_{j+1}-\frac{\bar{u}_{j+2}-2\bar{u}_{j+1}+\bar{u}_j}{24},\end{aligned}$$

and three indicators of smoothness $IS_j=((\bar{u}_{j-1}-\bar{u}_{j-2})^2+(\bar{u}_j-\bar{u}_{j-1})^2)/2+(\bar{u}_j-2\bar{u}_{j-1}+\bar{u}_{j-2})^2$, $IS_{j+1}=((\bar{u}_j-\bar{u}_{j-1})^2+(\bar{u}_{j+1}-u_j)^2)/2+(\bar{u}_{j+1}-2\bar{u}_j+\bar{u}_{j-1})^2$, and $IS_{j+2}=((\bar{u}_{j+1}-\bar{u}_j)^2+(\bar{u}_{j+2}-\bar{u}_{j+1})^2/2+(\bar{u}_{j+2}-2\bar{u}_{j+1}+\bar{u}_j)^2$. The reconstructed solution $R_j(x)$ will be a convex combination of $p_j'(x)$, $p_{j+1}'(x)$, and $p_{j+2}'(x)$; i.e.,

$$\begin{aligned}R_j(x)=&\frac{\alpha_0^j}{\alpha_0^j+\alpha_1^j+\alpha_2^j}p_j'(x)+\frac{\alpha_1^j}{\alpha_0^j+\alpha_1^j+\alpha_2^j}p_{j+1}'(x)\\ &+\frac{\alpha_2^j}{\alpha_0^j+\alpha_1^j+\alpha_2^j}p_{j+2}'(x),\end{aligned} \tag{3.18}$$

where $\alpha_0^j=C_0^j/(\varepsilon+IS_j)^3$, $\alpha_1^j=C_1^j/(\varepsilon+IS_{j+1})^3$, $\alpha_2^j=C_2^j/(\varepsilon+IS_{j+2})^3$. We shall specify C_0^j, C_1^j, and C_2^j in the following two cases:

Case 1. If $f'(\bar{u}_j)>0$, we choose $x_j^*=x_{j+1/2}$. We compute $a_0^j(x_{j+1/2})=6h^3$, $a_1^j(x_{j+1/2})=-2h^3$, and $a_2^j(x_{j+1/2})=2h^3$, and obtain $\eta_p=2$ and $\eta_n=1$; hence $C_0^j=\frac{1}{12}$, $C_1^j=\frac{1}{2}$, and $C_2^j=\frac{1}{4}$. Thus

$$\begin{aligned}\alpha_0^j&=\frac{1}{12(\varepsilon+IS_j)^3}\\ \alpha_1^j&=\frac{1}{2(\varepsilon+IS_{j+1})^3}\\ \alpha_{2k}^j&=\frac{1}{4(\varepsilon+IS_{j+2})^3}\end{aligned} \tag{3.19a}$$

in (3.18).

Case 2. If $f'(\bar{u}_j)\leqslant 0$, we choose $x_j^*=x_{j-1/2}$. We compute $a_0^j(x_{j-1/2})=-2h^3$, $a_1^j(x_{j-1/2})=2h^3$, and $a_2^j(x_{j-1/2})=$

$-6h^3$ and obtain $\eta_p = 1$ and $\eta_n = 2$; hence $C_0^j = \frac{1}{4}$, $C_1^j = \frac{1}{2}$, and $C_2^j = \frac{1}{12}$. Thus

$$\alpha_0^j = \frac{1}{4(\varepsilon + IS_j)^3}$$
$$\alpha_1^j = \frac{1}{2(\varepsilon + IS_{j+1})^3} \tag{3.19b}$$
$$\alpha_2^j = \frac{1}{12(\varepsilon + IS_{j+2})^3}$$

in (3.18).

4. NUMERICAL EXPERIMENTS

4.1. *Scalar Conservation Laws*

In this subsection we use some model problems to numerically test our schemes. We use the Roe flux with entropy fix as numerical flux and choose $r = 2$ which means we use a linear polynomial o reconstruct the solution and/or $r = 3$ which means we use a quadratic polynomial to reconstruct the solution, and we expect to achieve third- and fourth-order accuracy, respectively (at least away from sonic points), according to our analysis in the previous section.

EXAMPLE 1. We solve the model equation

$$\begin{aligned} &u_t + u_x = 0, && -1 \leqslant x \leqslant 1 \\ &u(x, 0) = u_0(x), && u_0(x) \text{ periodic with period 2.} \end{aligned} \tag{4.1}$$

Five different initial data $u_0(x)$ are used. The first one is $u_0(x) = \sin(\pi x)$ and we list the errors at time $t = 1$ in Table I. The second one is $u_0(x) = \sin^4(\pi x)$ and we list the errors at time $t = 1$ in Table II. Here and below l is the total number of cells and the step size $h = 2/l$ in all scalar examples.

TABLE I

$\tau/h = 0.8$, $t = 1$

l	L_1 error	L_1 order	L_∞ error	L_∞ order
$r = 2$				
80	2.77D-03		1.21D-02	
160	1.98D-04	3.81	1.11D-03	3.45
320	1.06D-05	4.22	4.30D-05	4.70
$r = 3$				
80	2.28D-05		1.03D-04	
160	9.65D-07	4.56	7.85D-06	3.71
320	1.71D-08	5.82	1.41D-07	5.80
640	6.07D-10	4.82	1.33D-09	6.73

TABLE II

$\tau/h = 0.8$, $t = 1$

l	L_1 error	L_1 order	L_∞ error	L_∞ order
$r = 2$				
80	1.77D-02		7.31D-02	
160	3.08D-03	2.52	1.86D-02	1.94
320	2.46D-04	3.65	2.04D-03	3.19
640	1.42D-05	4.11	9.28D-05	4.46
$r = 3$				
80	2.17D-03		6.87D-03	
160	1.13D-04	4.26	3.93D-04	3.91
320	3.71D-06	4.93	3.25D-05	5.21
640	6.39D-08	5.86	6.63D-07	5.62

For the first two initial data, we obtain about fourth- (for $r = 2$) and fifth- (for $r = 3$) order of accuracy, respectively, in the smooth regions in both L_1 and L_∞ norms which is surprisingly better than third- and fourth-order, the theoretical results. We note that standard ENO schemes applied to the example with the second initial data experienced an (easily fixed) loss of accuracy; see [6, 7]. No such degeneracy was found with our present methods.

The third initial function is

$$u_0(x) = \begin{cases} 1, & -\frac{1}{5} \leqslant x \leqslant \frac{1}{5}; \\ 0, & \text{otherwise,} \end{cases}$$

the fourth is

$$u_0(x) = \begin{cases} (1 - (\frac{10}{3}x)^2)^{1/2}, & -\frac{3}{10} \leqslant x \leqslant \frac{3}{10}, \\ 0, & \text{otherwise;} \end{cases}$$

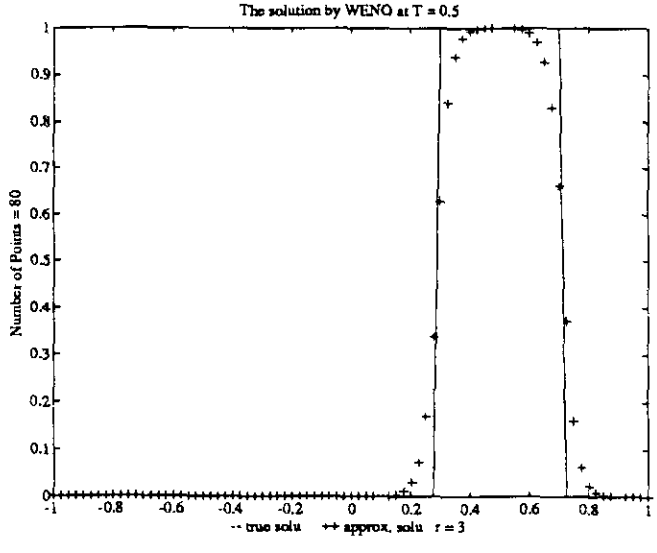

FIG. 1. $\tau/h = 0.8$.

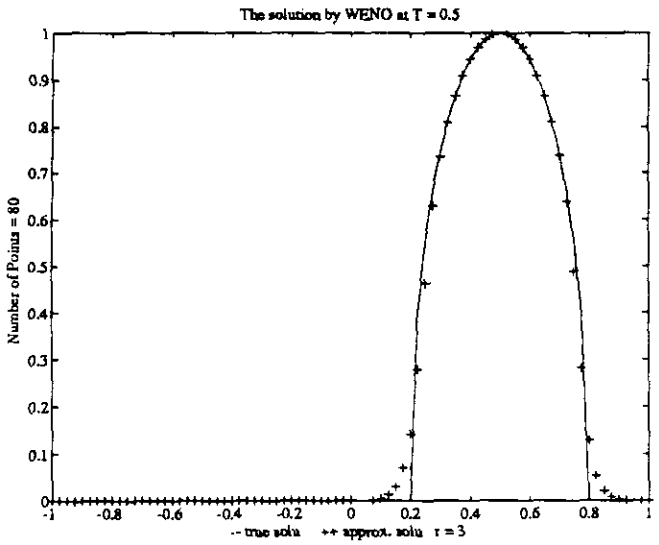

FIG. 2. $\tau/h = 0.8$.

and the fifth is

$$u_0(x) = e^{-300x^2}.$$

We see the good resolution of the solutions in Figs. 1–3 which are obtained by our scheme with $r = 3$. Linear discontinuities are smeared a bit. We expect to fix this in the future using either the subcell resolution technique of Harten [10] or the artificial compression technique of Yang [11] together with the present technique.

EXAMPLE 2. We solve Burgers' equation with a periodic boundary condition,

$$\begin{aligned} &u_t + (\tfrac{1}{2}u^2)_x = 0, \qquad -1 \leqslant x \leqslant 1 \\ &u(x, 0) = u_0(x), \qquad u_0(x) \text{ periodic with period 2.} \end{aligned} \tag{4.2}$$

TABLE III

$\tau/h = 0.6$, $t = 0.15$

l	L_1 error	L_1 order	L_∞ error	L_∞ order
$r = 3$				
80	2.63D-05		2.84D-04	
160	1.50D-06	4.13	2.68D-05	3.41
320	5.44D-08	4.79	3.63D-07	6.21

For the initial data $u_0(x) = \frac{1}{2} + \sin(\pi x)$, the exact solution is smooth up to $t = 1/\pi$; then it develops a moving shock which interacts with a rarefaction wave. Observe that there is a sonic point.

At $t = 0.15$ the solution is still smooth. We list the errors in Table III. Note that we also have about fifth- (for $r = 3$) order of accuracy respectively both in L_1 and L_∞ norms.

At $t = 1/\pi$ the shock just begins to form; at $t = 0.55$ the interaction between the shock and the rarefaction waves is over and the solution becomes monotone between shocks. In Figs. 4–5 which are obtained by our scheme with $r = 3$ we can see the excellent behavior of the schemes in both cases. The errors at a distance 0.1 away from the shock (i.e., $|x - \text{shock location}| \geqslant 0.1$) are listed in Table IV at $t = 0.55$. These errors are of same magnitude as the ones in the smooth case of Table III show about fifth- (for $r = 3$) order of accuracy respectively both in L_1 and L_∞ in the smooth regions 0.1 away from the shock. This shows that the error propagation of the schemes is still very local.

EXAMPLE 3. We use two nonconvex fluxes to test the convergence to the physically correct solutions. The true solutions are obtained from the Lax–Friedrichs scheme on

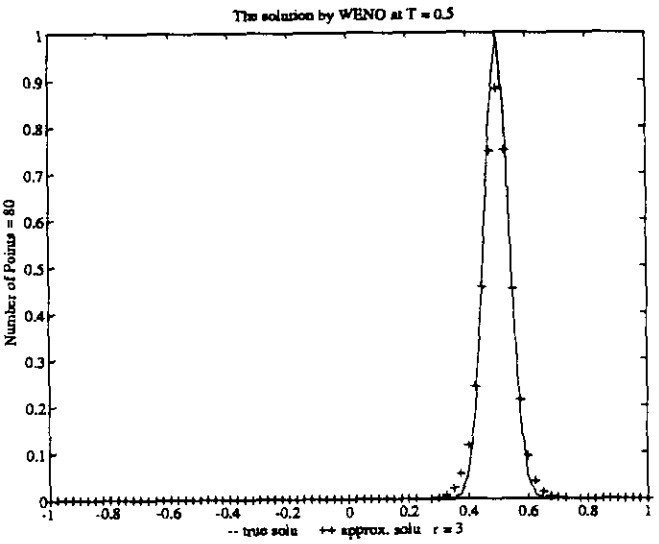

FIG. 3. $\tau/h = 0.8$.

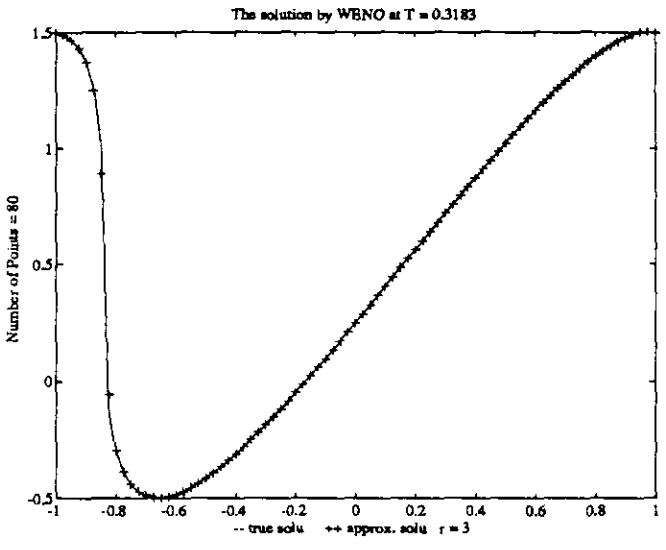

FIG. 4. $\tau/h = 0.6$.

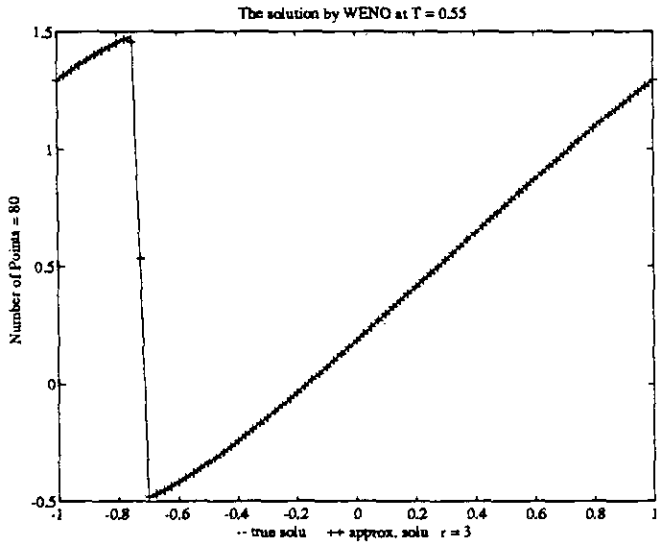

FIG. 5. $\tau/h = 0.6$.

a very fine grid. We use our scheme with $r = 3$ in this example. The first one is a Riemann problem with the flux $f(u) = \frac{1}{4}(u^2 - 1)(u^2 - 4)$ and the initial data

$$u_0(x) = \begin{cases} u_l, & x < 0 \\ u_r, & x > 0. \end{cases}$$

The two cases we test are (i) $u_l = 2$, $u_r = -2$, Fig. 6; (ii) $u_l = -3$, $u_r = 3$, Fig. 7. For more details concluding this problem see [2].

The second flux is the Buckley–Leverett flux used to model oil recovery [2], $f(u) = 4u^2/(4u^2 + (1-u)^2)$, with initial data $u = 1$ in $[-\frac{1}{2}, 0]$ and $u = 0$ elsewhere. The result is displayed in Fig. 8. In this example, we observe convergence with good resolution to the entropy solutions in both cases.

In all the examples that we have illustrated above, we observe that the schemes are of about fourth- (for $r = 2$) and fifth- (for $r = 3$) order of accuracy, respectively, and convergent with good resolution to the entropy solutions.

TABLE IV

$\tau/h = 0.6$, $t = 0.55$

l	L_1 error	L_1 order	L_∞ error	L_∞ order
$r = 3$				
80	2.29D-05		7.63D-04	
160	7.71D-07	4.89	3.83D-05	4.32
320	7.41D-09	6.70	7.27D-07	5.72

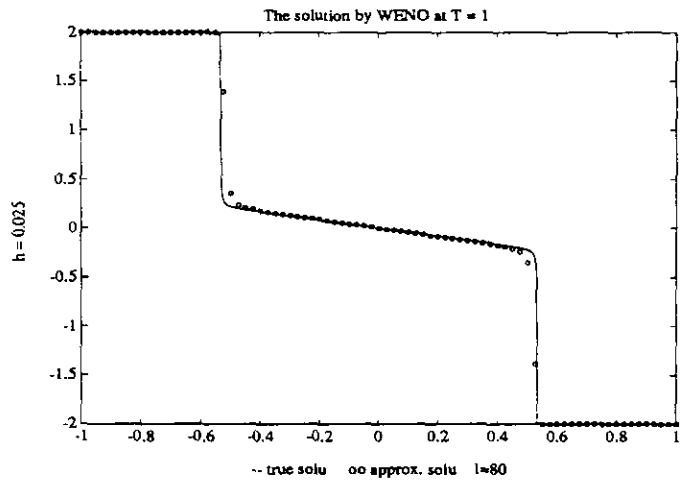

FIG. 6. $\tau/h = 0.3$.

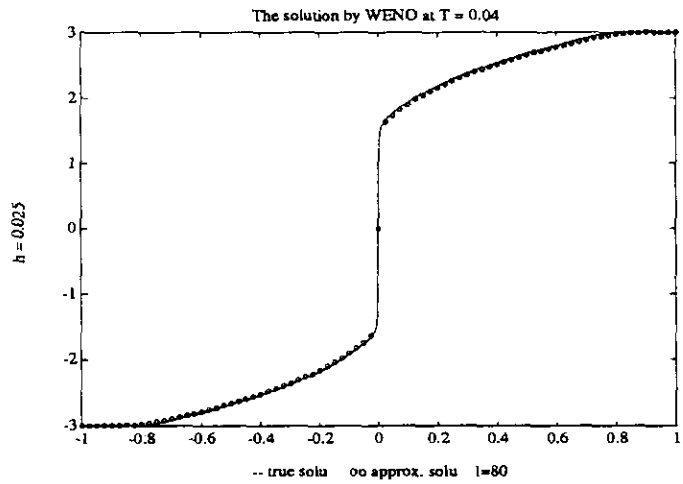

FIG. 7. $\tau/h = 0.04$.

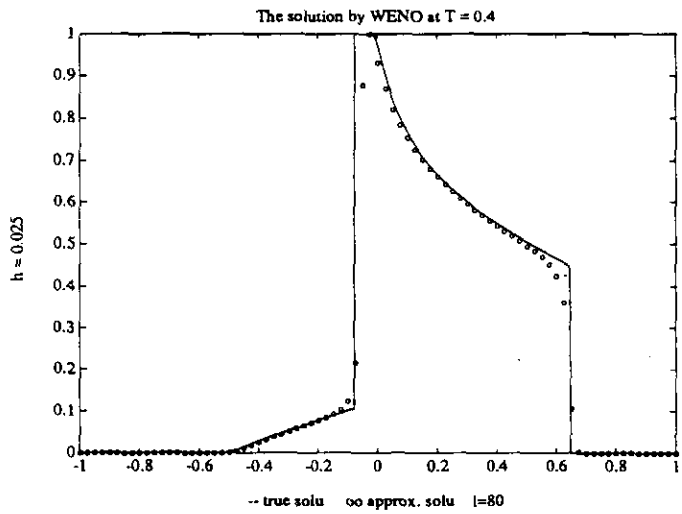

FIG. 8. $\tau/h = 0.4$.

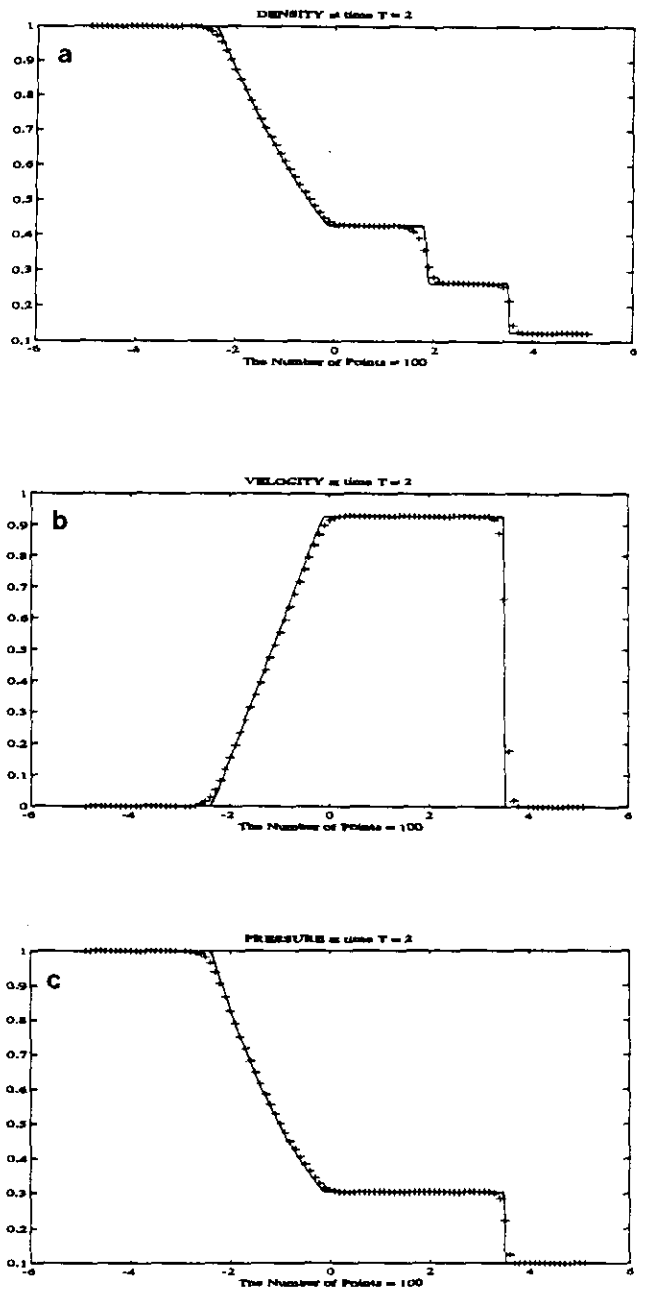

FIG. 9. (a) $\tau/h = 0.4$, $t = 2$; (b) $\tau/h = 0.4$, $t = 2$; (c) $\tau/h = 0.4$, $t = 2$.

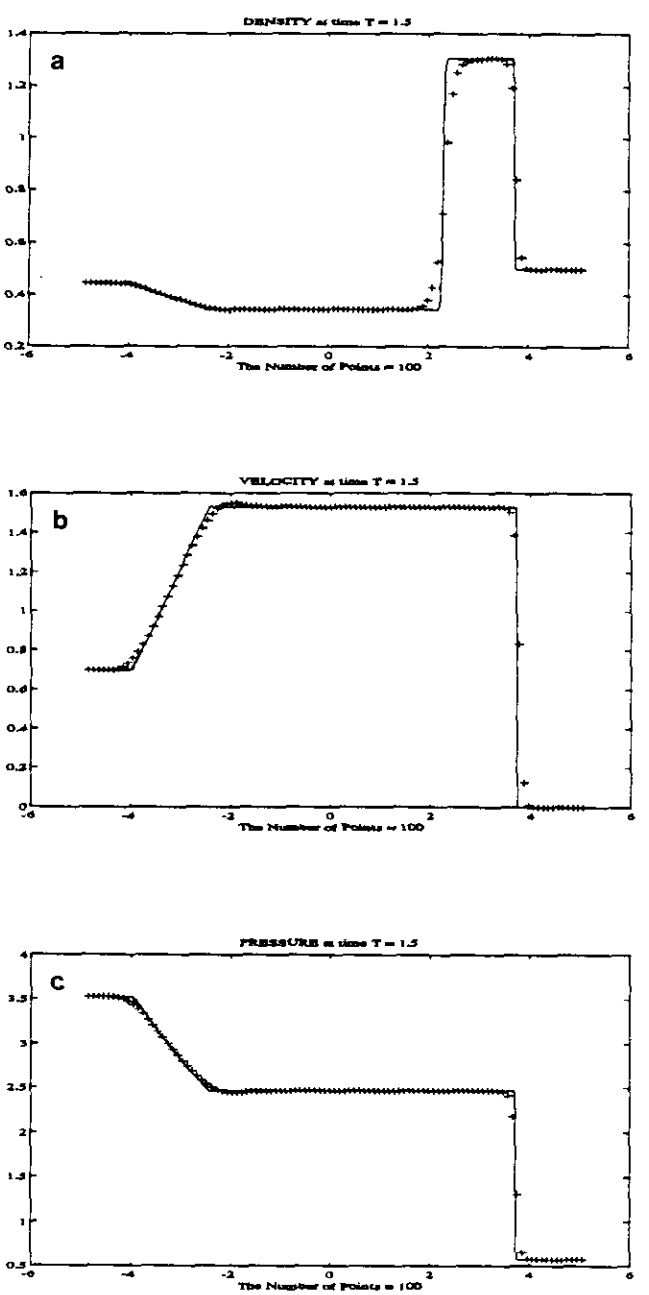

FIG. 10. (a) $\tau/h = 0.2$, $t = 1.5$; (b) $\tau/h = 0.2$, $t = 1.5$; (c) $\tau/h = 0.2$, $t = 1.5$.

TABLE V

$\tau/h = 0.6$, $t = 1$

l	L_1 error	L_1 order	L_∞ error	L_∞ order
Density				
80	1.99D-04		1.29D-03	
160	1.21D-05	4.03	1.15D-04	3.49
320	1.74D-07	6.12	2.07D-06	5.80
640	2.92D-09	5.90	3.20D-08	6.02
Momentum				
80	2.17D-04		1.76D-03	
160	1.29D-05	4.07	1.50D-04	3.55
320	1.85D-07	6.12	2.43D-06	5.95
640	3.09D-09	5.90	3.20D-08	6.25
Energy				
80	2.10D-04		1.92D-03	
160	1.19D-05	4.14	1.60D-04	3.59
320	1.55D-07	6.26	2.57D-06	5.96
640	2.75D-09	5.82	3.10D-08	6.37

4.2. *Euler Equations of Gas Dynamics*

In this subsection we apply our schemes to the Euler equation of gas dynamics for a polytropic gas,

$$\begin{aligned} &u_t + f(u)_x = 0 \\ &u = (\rho, m, E)^{\mathrm{T}} \\ &f(u) = qu + (0, P, q^P)^{\mathrm{T}} \\ &P = (\gamma - 1)(E - \tfrac{1}{2}\rho q^2) \\ &m = \rho q, \end{aligned} \tag{4.2}$$

where $\gamma = 1.4$ in the following computation. For details of the Jacobian, its eigenvalues, eigenvectors, etc., see [2].

EXAMPLE 4. We consider the following Riemann problems:

$$u_0(x) = \begin{cases} u_l, & x < 0 \\ u_r, & x > 0. \end{cases}$$

Two sets of initial data are used. One is proposed by Sod in [8]:

$$(\rho_l, q_l, P_l) = (1, 0, 1), \qquad (\rho_r, q_r, P_r) = (0.125, 0, 0.1).$$

The other is used by Lax [9]:

$$(\rho_l, q_l, P_l) = (0.445, 0.698, 3.528),$$
$$(\rho_r, q_r, P_r) = (0.5, 0, 0.571).$$

We test our schemes with $r = 3$. We use the characteristic reconstruction and Roe flux with the entropy fix formed by Roe's average as the numerical flux. For details see [2]. The results are displayed in Figs. 9 and 10.

EXAMPLE 5. In this example we shall test the accuracy of our schemes ($r = 3$) for the Euler equation of gas dynamics for a polytropic gas. We choose initial data as $\rho = 2 + \sin(\pi x)$, $m = 2 + \sin(\pi x)$, and $E = 2 + \sin(\pi x)$, and the periodic boundary condition. The true solution was obtained by applying the schemes to a very fine grid. For time $t = 1$ when shocks have not formed, our schemes

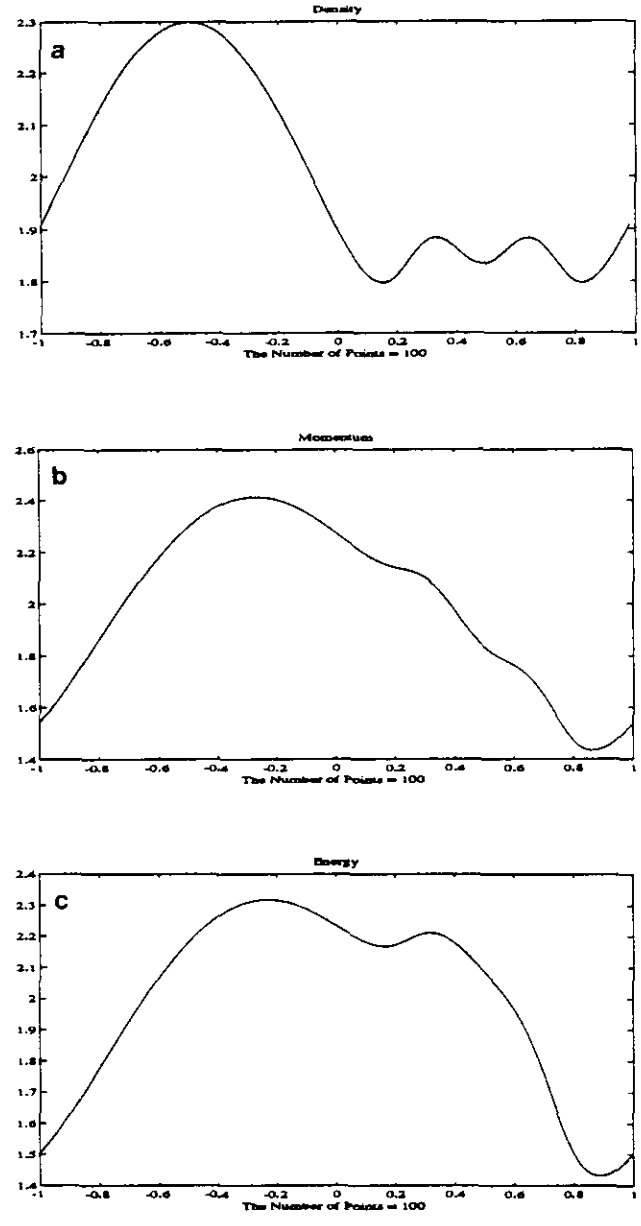

FIG. 11. (a) $\tau/h = 0.6$, $t = 1$; (b) $\tau/h = 0.6$, $t = 1$; (c) $\tau/h = 0.6$, $t = 1$.

achieve fifth- ($r = 3$) order accuracy in all three components, see Table V. We can also see the solution for time $t = 1$ in Fig. 11.

ACKNOWLEDGMENT

We are grateful to Professor Chi-Wang Shu for his suggestion of the smooth indicator function, i.e.,

$$IS_j = \sum_{l=1}^{r-1} \left(\sum_{k=1}^{l} (\Delta^{r-l}[u_{j-r+k}])^2 \right) / l,$$

instead of

$$IS_j = \sum_{l=1}^{r-1} \left(\sum_{k=1}^{l} |\Delta^{r-l}[u_{j-r+k}]| \right) / l,$$

which we used originally. Both functions work well; however, the latter one leads to a smoother (C^∞ vs. Lipschitz) numerical flux which may be helpful for steady state convergence or convergence proof.

REFERENCES

1. A. Harten and S. Osher, *SIAM J. Numer. Anal.* **24**, 279 (1987); MRC Technical Summary Report No. 2823, May 1985 (unpublished).
2. A. Harten, B. Engquist, S. Osher, and S. Chakravarthy, *J. Comput. Phys.* **71**, 231 (1987); ICASE Report No. 86-22, April 1986 (unpublished).
3. C.-W. Shu and S. Osher, *J. Comput. Phys.* **77**, 439 (1988).
4. C.-W. Shu and S. Osher, *J. Comput. Phys.* **83**, 32 (1989).
5. A. Harten and S. Chakraverthy, UCLA CAM Report No. 91-16, August 1991 (unpublished).
6. A. Rogerson and E. Meiburg, *J. Sci. Comput.* **5** (2), 151 (1990).
7. C.-W. Shu, *J. Sci. Comput.* **5** (2), 127 (1990).
8. G. Sod, *J. Comput. Phys.* **27**, 1 (1978).
9. P. Lax, *Commun. Pure Appl. Math.* **46**, 1 (1986).
10. A. Harten, *J. Comput. Phys.* **83**, 148 (1989).
11. H. Yang, *J. Comput. Phys.* **89**, 125 (1190).